



Application of novel organic acid-modified biosorbent in the sequestration of aqueous zinc ion

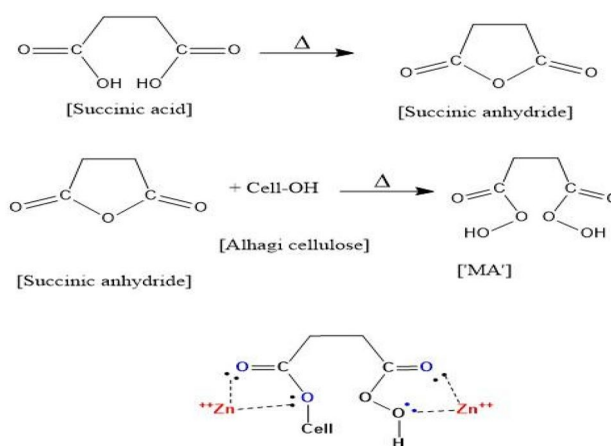
Chukwunonso Onyeka Aniagor¹ · Doaa Mohamed Hussein² · Sohair Farag³ · Ali Hashem³

Received: 7 November 2021 / Accepted: 14 March 2023 / Published online: 31 March 2023
© The Author(s), under exclusive licence to Springer Nature Switzerland AG 2023

Abstract

Alhagi graecorum (AG) is an invasive plant with a massive/robust root structure that can grow up to 12 feet into the ground. The present study exploited the rich cellulosic content in this 'AG' root for the synthesis of a novel biosorbent ('MA'). This low-cost biosorbent, with high carboxyl content of 447.22 (m eq/100 g sample) was utilized for aqueous zinc ion sequestration. The surface functional groups and textural characteristics required for an efficient heavy metal binding were identified on 'MA' using Fourier transform infrared spectroscopy and scanning electron microscopy. Sip isotherm emerged as the model of best fit for equilibrium studies; hence, Zn (II) ion sorption onto 'MA' is believed to occur via a hybrid blend of homogeneous monolayer and heterogeneous multilayer adsorption. Meanwhile, the Elovich (SNE = 1.0429), intraparticle diffusion (SNE = 1.0205) and pseudo-first order (SNE = 1.0455) provided the best fitting for 200, 400 and 600 mg/L adsorption system, respectively. The maximum adsorption capacity of 188.67 mg/g was recorded at optimum adsorption conditions, with the predominance of the electrostatic and electron donor–acceptor interaction mechanism. The abundant surface oxygenous functional groups on 'MA' positively influenced its adsorption capacity, thus making it a promising biosorbent for aqueous Zn (II) uptake.

Graphical abstract



Keywords Adsorption · Zinc ion · Biosorbent · Adsorption mechanism · Adsorption modelling

✉ Chukwunonso Onyeka Aniagor
co.aniagor@unizik.edu.ng

✉ Ali Hashem
alhashem2000@yahoo.com

Extended author information available on the last page of the article

Introduction

Zn(II) is an essential elemental requirement for healthy living, especially when it is retained in the body in an appropriate concentration (Jagaba et al. 2020). A maximum

permissible limit of 5 mg/L was stipulated by the World Health Organization (WHO) and the United States Environmental Protection Agency (USEPA) for Zn(II) in drinking water (Jagaba et al. 2020). However, any aqueous concentration higher than the aforementioned limit could result in varying degrees of health challenges (Wołowiec et al. 2019; Barakat 2011). Accordingly, zinc ion contamination occurs mainly via inappropriate disposal of effluents from chemical process industrial into the aquatic environment (Badruddoza et al. 2013; Chen et al. 2018) and their efficient removal often poses a serious challenge to researchers and the scientific community.

Several technologies (Wołowiec et al. 2019; Badruddoza et al. 2013; Awual et al. 2019a; Matouq et al. 2015) have been applied for heavy metal uptake from an aqueous environment. However, some of these technologies have associated limitations, like low treatment efficiency, high energy and cost requirement, non-eco-friendly, etc. (Awual 2016; Awual et al. 2019b; Shahat et al. 2018a, b). In this work, the use of locally sourced biosorbent was explored for the uptake of aqueous zinc ions. The preference for the biosorption approach is related to its operational flexibility, process efficiency, efficient regeneration of spent adsorbent, etc. (Awual et al. 2017; Al-Shaalan et al. 2019; Ali et al. 2019, 2018).

Consequently, a variety of biosorbents, such as fungal mycelial wastes (Luef et al. 1991), rice bran (Wang et al. 2006), *Azadirachta indica* bark (King et al. 2008), immobilized *Candida utilis* and *Candida tropicalis* cells (Ahmad et al. 2013) and rapeseed waste (Paduraru et al. 2015), have been successfully applied for aqueous zinc ion uptake. Also, the *Eichhornia crassipes* biomasses were successfully applied for the uptake of copper ions (Komy et al. 2013; Abdelraheem et al. 2017, 2016). Fadzil et al. (2016) evaluated the Pb(II) sorption capacities of rubber leaf powder modified with citric acid and monosodium glutamate. The modification involves the esterification of the respective organic acids onto the cellulose structure of the precursor. The study noted that the organic acid modifier improved the biosorbents' effectiveness at removing the aqueous Pb(II) ions. Similarly, citric acid-modified cellulose nanofibrous mats with reasonably high absorption selectivity for Cr(VI) was successfully prepared by Zhang et al. (2020). The authors reported that the nanoscale biomass materials showed great potential for removing heavy metals from wastewater. The adsorption capacity of natural sawdust towards Pb(II) ions was considerably enhanced due to the introduction of carboxylic groups on their surface via organic acid modification (Salazar-Rabago and Leyva-Ramos 2016). Thus, the adsorption capacity was also found to be linearly dependent on the concentration of carboxylic sites. Ranasinghe et al. (2018) investigated the heavy metal adsorption potentials of organic acid-modified Jackfruit peel.

Using ethylenediaminetetraacetic acid (EDTA) and sodium dodecyl sulphate (SDS) as the modifiers, excellent adsorption characteristics for Cr(III) and Ni(II) were recorded.

Alhagi graecorum is an invasive tropical plant that often serves as animal fodder, but its elimination from invaded farmland could be very challenging (Ebrahimi et al. 2015). Considering its invasiveness, relative availability and rich cellulosic content, *Alhagi graecorum* adoption as the choice of adsorbent precursor in this study is justified. The novel biosorbent ('MA') was obtained through dual reaction stages of direct carbonylation of hydroxyl groups, -OH (using succinic acid) and subsequent esterification of the resultant anhydride analogue into ester of high carboxyl (-COOH) content. The characteristics of the biosorbent precursor and its modifier are complementary in certain ways. The *Alhagi graecorum* plant is readily available and can be accessed at no cost. However, it has limited carboxyl groups; hence, its poor metal ion sorption capacity. Conversely, the esterification agent (succinic acid) is a liquid and cannot be applied as a sole adsorbent. The aqueous zinc ion sorption ability of the novel biosorbent was subsequently evaluated under batch mode. The surface chemistry, elemental distribution and morphological features of the synthesized adsorbent were obtained, while the effect of various process variables on the adsorption capacity was elucidated in this study.

Materials and methods

Materials

The *Alhagi graecorum* (AG) plant was obtained from the Matrouh desert, Egypt. The root of this plant was separated from the stems and leaves, and the latter was discarded. The root material was carefully washed with distilled water to remove every adherent earth particle and then oven-dried at 80 °C for 10 h. The dried root material was subsequently ground and sieved to a particle size of 50–125 µm. All reagents used in this study, zinc acetate (100–800 mg/L), EDTA (0.0005 M), succinic acid (16.94 mmol/l), acetic acid (10%), sodium carbonate (1N), acetone (≥ 99.99% purity) and ethyl alcohol (> 99% purity), were all laboratory-grade chemicals, supplied by Merck, Germany.

Preparation of the adsorbent

The novel adsorbent (MA) was synthesized as follows: 2 g of the *Alhagi graecorum* (AG) powder was added to a beaker containing an aqueous solution of succinic acid (16.94 mmol/l) whose volume is sufficient enough to achieve a slurry. The mixture was manually stirred using a spatula to achieve homogeneity. Afterwards, the homogeneous slurry was oven-dried (at 100–150 °C) and subsequently cooled to

room temperature to obtain 'MA'. The dried 'MA' sample was washed with ethanol/water solution (80:20) to get rid of any unreacted acid/soluble by-products, followed by oven-drying at 80 °C for 6 h. The adsorbent synthesis stages are concisely represented in Fig. 1.

Adsorbent characterization

The IR spectra were recorded at the wavelength range of 4000–400 cm^{-1} using Perkin-Elmer, Shimadzu FTIR-8400S spectrophotometer. The SEM micrograph was obtained using a Scanning Electron Microscope, Model JEOL-JSM-5600 (operating at an accelerating voltage of 25.00 kV). The energy dispersive X-ray (EDX) mapping detector (Model JEOL-JSM-5600) attached to the SEM equipment was used for studying the biosorbents' elemental distribution. The point of zero charge (pH_{pzc}) of the biosorbent was obtained following the procedure earlier reported by Khalil et al. (1990) and Noh and Schwarz (1990).

Carboxyl content estimation

The carboxyl content of 'MA' was determined following the procedure reported in our earlier work (Hashem et al. 2021). Meanwhile, the percentage of carboxyl content was subsequently evaluated using Eq. (1).

$$[\text{COOH}]_{\text{m eq/100 g sample}} = \frac{(V_0 - V_1)N}{W} \times 100, \quad (1)$$

where V_0 = Volume of HCl consumed for the blank experiment (mL), V_1 = HCl volume (mL) consumed by the adsorbent sample, N = normality of the HCl solution and W = mass of the 'MA' (g).

Batch adsorption studies

A specific amount of 'MA' (0.3 g) was contacted with 100 mL of a Zn (II) ion solution in a 125 mL Erlenmeyer flask. The solution pH was rightly tuned using either 0.1 M HNO_3 or 0.1 M NaOH. After a certain period of agitation (at 150 rpm, 30 °C), the mixture was filtered using Whatman No. 41 paper to separate the adsorbent and metal ion solution. The variation in the Zn (II) ion concentration was obtained from the direct titration with a standard EDTA solution. The effect of process variables on the 'MA' adsorption capacity was conducted by varying the agitation time from 0 to 180 min, adsorbent mass from 0.3 to 7.0 g/L and adsorbate solution temperature from 30 to 60 °C. Meanwhile, the relevant parameters (amount adsorbed at equilibrium, q_e , and removal efficiency, R.E %) derivable from the adsorption experiment were evaluated with Eqs. (2)–(3). For the avoidance of experimental error, a duplicate version of the respective batch adsorption and effect of process variable experiments were conducted and the accurate mean values for q_e were obtained in each case:

$$q_e = \frac{(C_0 - C_e)V}{W}, \quad (2)$$

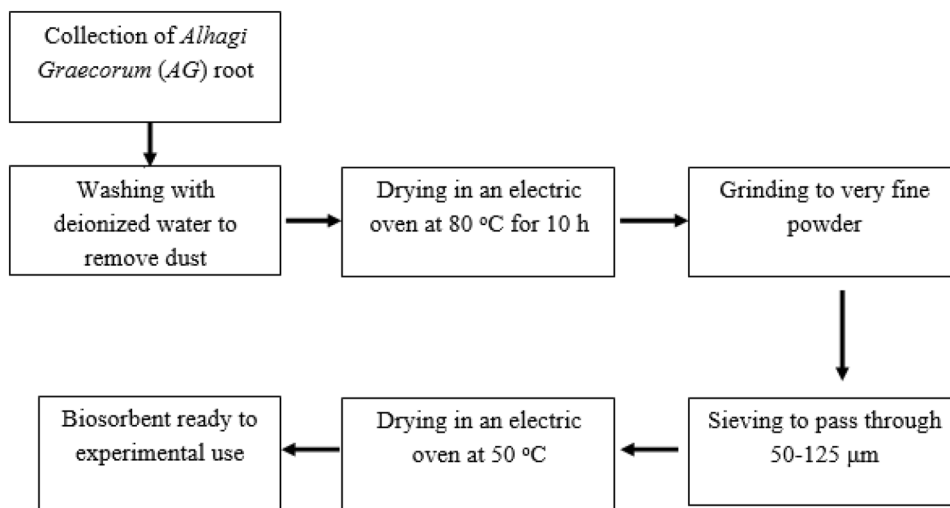
$$\text{RE (\%)} = \frac{C_0 - C_e}{C_0} \cdot 100\%, \quad (3)$$

where C_0 = Initial Zn (II) concentration (mg L^{-1}), C_e = Zn (II) concentration at equilibrium (mg L^{-1}), W = adsorbent mass (g) and V = volume of Zn (II) solution used (L).

Adsorption modelling

Insight into the adsorbate–adsorbent interaction during the adsorption process is obtained from adsorption isotherm

Fig. 1 Flowchart for the biosorbent synthesis



modelling, while the various model parameters could inform the probable sorption mechanism (Vargas et al. 2012; Abonyi et al. 2019; Menkiti et al. 2018a). The experimental equilibrium data generated from this study were modelled with the non-linear form of Langmuir (Langmuir 1916; Hashem et al. 2020a, 2016), Freundlich (Freundlich 1907; Ighalo et al. 2020; Igwegbe et al. 2020a), Temkin (Menkiti et al. 2018b; Temkin 1940), D-R (Foo and Hameed 2010; Hashem et al. 2020b), Khan (Khan et al. 1997; Aniagor and Menkiti 2020), Redlich-Peterson (Redlich and Peterson 1959; Menkiti and Aniagor 2018), Toth (Toth 1971; Schweitzer and Noblet 2018) and Sips (Aniagor and Menkiti 2020; Yan et al. 2019) models. The mathematical expression of these isotherm models is presented in supplementary Table 1 (Table S1). Similarly, the dynamics and kinetics involved in the present sorption process were studied using pseudo-first-order (Hashem and Badawy 2015; Aniagor and Menkiti 2018), pseudo-second-order (Aniagor and Menkiti 2019; Hashem et al. 2011), Elovich (Menkiti et al. 2018b), intraparticle diffusion (Menkiti et al. 2018a; Hashem et al. 2020c) and Bangham (Aniagor and Menkiti 2018) kinetic models. The kinetic model equations are also presented in Table S2.

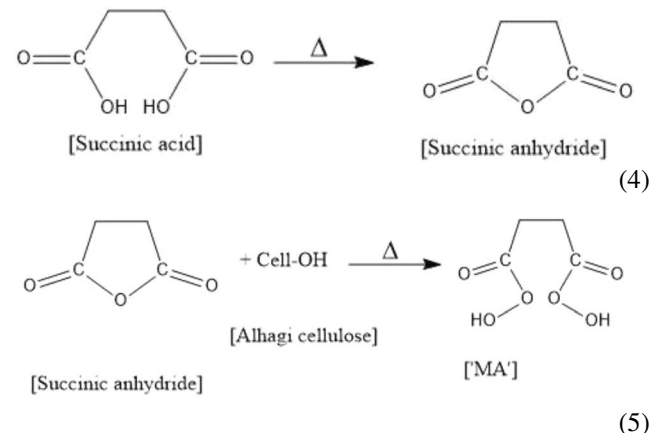
The non-linear model goodness of data fit is usually evaluated from the magnitude of some dedicated goodness-of-fit (GO-Fm) models. The goodness-of-fit evaluation is made based on the following criteria: (1) the lower the error values for a given isotherm or kinetic model, the better the model fit, and (2) the larger the R^2 -value the better the model fit. The GO-Fm models applied in this work comprising average relative error, ARE (Marquardt 1963), average percentage error, APE (Khair et al. 2017), the sum of squared error, SSE (Ng et al. 2002), hybrid fraction error, HYBRID (Kapoor and Yang 1989), Marquardt's Percent Standard Deviation, MPSD (Marquardt 1963), Non-linear chi-square test, χ^2 (Rivas et al. 2006) and Coefficient of determination, R^2 (Kumar et al. 2008). The equation of these GO-Fm models is presented in Table S3.

Results and discussion

Reaction mechanisms involved during adsorbent synthesis

The novel adsorbent ('MA') was synthesized following the procedure presented in "Preparation of the adsorbent". The reaction mechanism involved during the synthesis process is elucidated herein. The heat treatment involved during the oven-drying of the succinic acid-impregnated *Alhagi graecorum* powdered (AG) catalysed the direct carbonylation of the succinic acid to its corresponding anhydride according to Eq. (4). The acid anhydride groups further reacted with the

hydroxyl groups of 'AG' (Cell-OH) via partial or complete esterification to produce mono- or di-ester, respectively of high carboxyl content, which is the desired novel adsorbent ('MA') [as shown in Eq. (5)]. The carboxyl content of the synthesized 'MA', as evaluated from Eq. (1) is 447.22 (m.eq /100 g sample) at optimum reaction conditions. The factors that affected the carboxyl yield during the biosorbent synthesis are further discussed in sub "Effect of adsorbent synthesis process variables".

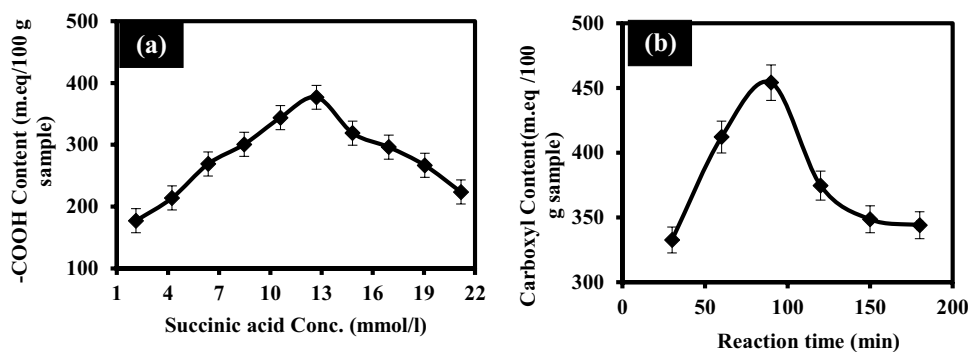


Effect of adsorbent synthesis process variables

Effect of succinic acid concentration The variation of the succinic acid concentration and the biosorbents' carboxyl content is shown in Fig. 2a. The -OH groups of the biosorbent precursor are considered the limiting reactant during the synthesis process. Therefore, the more readily the organic acid groups reach and interact with them, the more the carboxyl group formation. This could be the reason for the observed increment in the carboxyl content on the 'MA' the succinic acid concentration initially increased (see Fig. 1a). Meanwhile, at much higher acid concentrations, the unavailability or probable exhaustion of formally available hydroxyl groups of the precursor material may cause the dissociation of already existent carboxyl groups, thus the observed carboxyl content reduction (Fig. 2a).

Effect of dehydration time The variation of the succinic acid concentration and the biosorbents' carboxyl content is shown in Fig. 2b. The plot depicted a steady increment in 'MA' carboxyl content with a dehydration time of up to 90 min. However, further extension of the dehydration time (beyond 90 min) caused a decline. It is believed that as the dehydration time increased from 30 to 90 min, there was adequate predisposal time for achieving an optimal esterification reaction between the hydroxyl groups of the cellulosic biomass and the anhydride analogue of the succinic acid. However, when the duration of dehydration extended beyond 90 min, there was a reduction in the rate of esterifi-

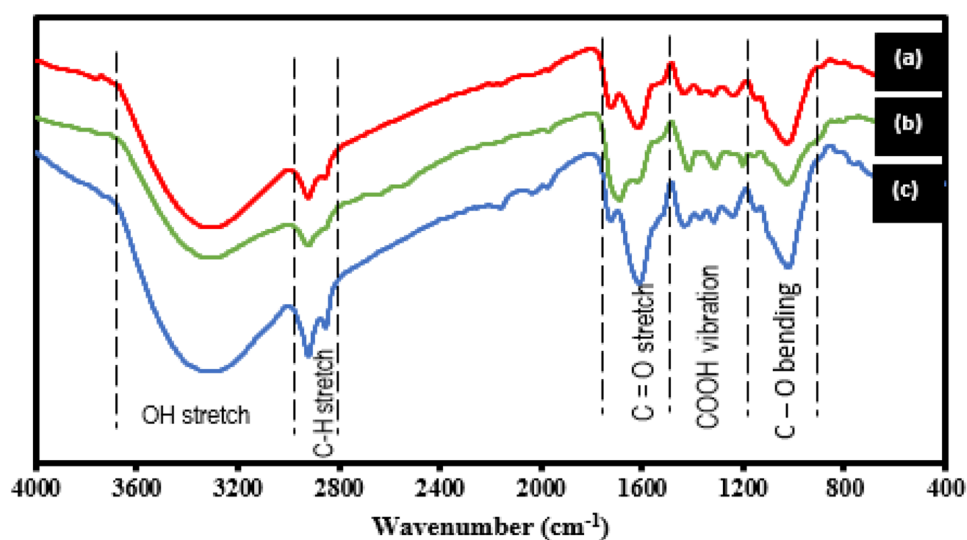
Fig. 2 The effect of **a** succinic acid concentration and **b** dehydration time on the carboxyl content of 'MA' (error bars represent \pm standard experimental errors)



cation due to the exhaustion of the esterification sites on the adsorbent. Also, the surrounding ligands could constitute some form of steric hindrance and such an effect is detrimental to the rate of esterification reaction. The deprotonation of the available carboxyl groups (decarboxylation) due to the possible formation of a zwitterionic tautomer (Serguchev and Beletskaya 1980) could also be responsible for the decreased carboxyl content.

Huang et al. (2018) and Zhou et al. (2018) also synthesized a novel adsorbent with abundant carboxyl groups through esterification reactions involving citric acid (CA) crosslinked β -cyclodextrin (CD) polymer (CD/CA). Instead of the thermal catalysation approach adopted in the present study, the esterification reaction reported in the aforementioned studies was catalysed using potassium dihydrogen pyrophosphate (KH_2PO_4). Similarly, Sayahi and Asadabadi (2022) and Li et al. (2017), respectively, prepared carboxylated cellulose from pineapple peel cellulose and softwood pulp via one-pot esterification and hydrolysis reaction. The synthesis protocol of both authors was similar to those adopted in this study but with different organic acids. Furthermore, the reaction product obtained by Li et al. (2017) was dehydrated at 110 °C within a time range of 15–120 min.

Fig. 3 FTIR spectra for **a** Zn (II)-loaded 'MA', **b** 'MA', **c** raw Alhagi



Adsorbent characterization

Fourier transform infrared spectroscopy (FTIR)

The FTIR spectra of the raw (AG), modified (MA) and metal-loaded [Zn (II)-MA'] biosorbent together with their observed peaks are presented in Fig. 3. Similar peaks were observed for the biosorbent samples, except for some slight wavenumber shifts, peak broadening or shrinking etc sequel to functionalization and heavy metal loading. The prominent peaks identified at 3333, 2916, 2844, 1719–1610 and 1512 cm^{-1} are assigned to the O–H stretching vibration, symmetric C–H stretch, asymmetric C–H stretch, aromatic C=O group of ester and lignin C–O linkage, respectively (Adigun et al. 2019). The peaks domicile at 1423 and 1228 cm^{-1} are typical of the asymmetric –COOH stretch of cellulose and hemicellulose. Also, a signature bending vibration band of the C–O group is assigned to the peak at wavenumber 1024 cm^{-1} (Sasmal et al. 2012). Meanwhile, the post-adsorption FTIR pattern is characterized by variations in peak length and intensities (Fig. 3).

Scanning electron microscopy (SEM)

The raw Alhagi (Fig. 4a) depicted a textural characteristic of thin, paper-like overlapped structures, with some degree of surface roughness and poorly developed pores. After undergoing the functionalization stages of acid and heat treatment, the 'MA' surface significantly transformed and depicted well-developed pores and increased surface roughness (Fig. 4b). Upon further comparison of the pre- and post-adsorption image of 'MA' (Figs. 4b, c), the only obvious identified distinction is that the surface of Zn (II)-loaded 'MA' depicted a characteristic lustre. This could probably be due to the presence of the adsorbed zinc ion.

The EDX elemental mapping was performed to confirm the presence of adsorbed zinc ions and also to ascertain their percentage deposition. As shown in Fig. 5, the presence of carbon (66.97%), oxygen (28.81%) and Zinc (4.22%) was detected in the post-adsorption 'MA' sample. This finding

serves as a confirmation of the uptake of Zinc ions by 'MA' via the adsorption process.

Adsorption performance of 'MA'

Effect of pH

It has been reported that the surface charge of a given adsorbent is a function of the adsorbate solution pH and its (biosorbents') point of zero charges, pH_{PZC} . According to Fig. 6a, the 'MA' depicted a pH_{PZC} of pH 4.1, an indication of its surface acidity nature. The assertion was further corroborated by the presence of carboxylic functional groups identified from the FTIR spectra. Meanwhile, Eqs. (6) and (7) present the stoichiometric illustration of the ion exchange/electrostatic interaction mechanism occurring within the zinc ion sorption system. These equilibrium reactions are strongly dependent on the pH of the adsorbate solution. At strongly acidic conditions ($pH < pH_{PZC}$)

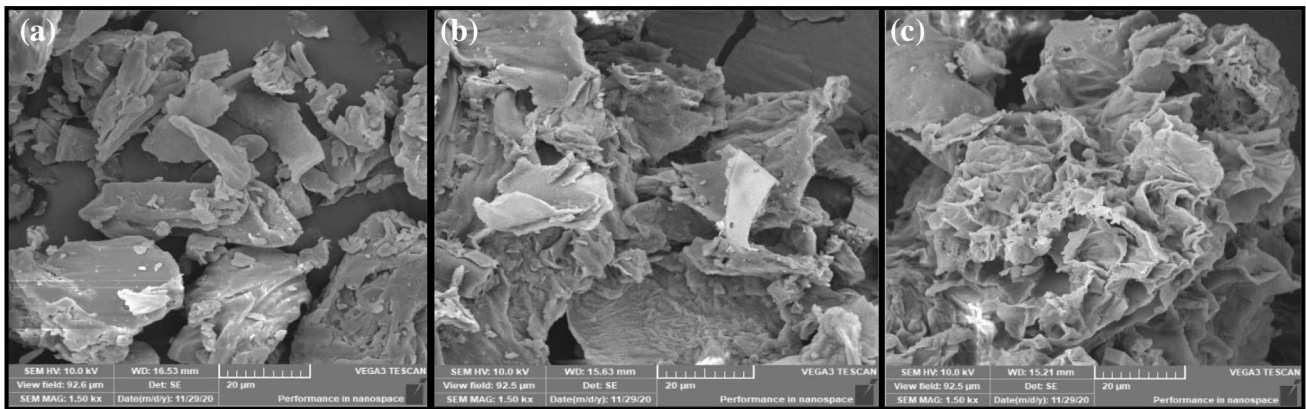


Fig. 4 SEM images of **a** raw Alhagi, **b** 'MA', **c** Zn (II)-loaded 'MA'

Fig. 5 EDX spectra for Zn (II)-loaded 'MA'

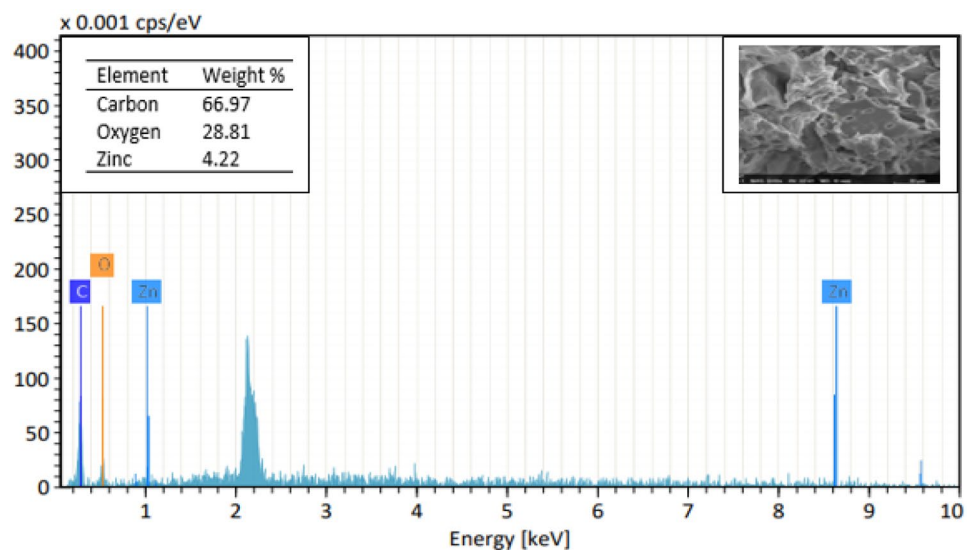
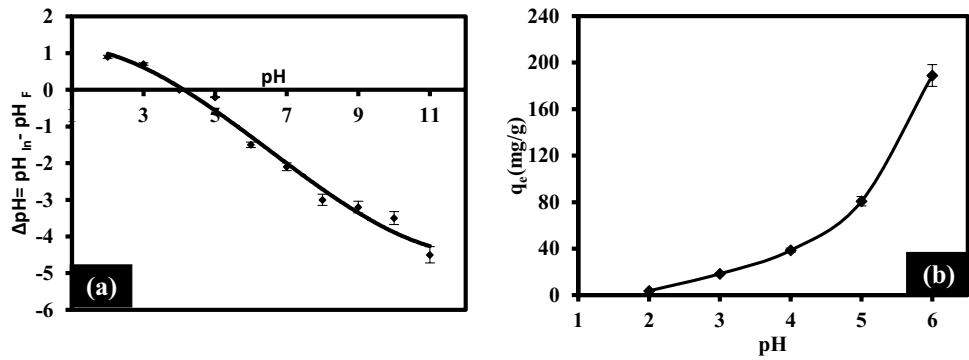
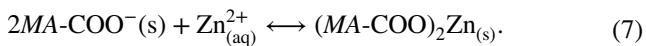
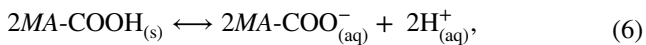


Fig. 6 Plot of the **a** pH of point of zero charge, **b** effect of pH on the adsorption capacity (error bars represent \pm standard experimental errors)



the backward reaction of Eq. (6) is favoured, thus the predominance of the carboxylic groups on the adsorbent in its non-ionized form. A typical scenario was observed at pH 2.0 (Fig. 6b), where no notable adsorption capacity value was recorded, due to a strong electrostatic repulsion between the zinc cations and protonated adsorbent surfaces.



Subsequent deprotonation of the adsorption sites as shown in Eq. (7) due to a decrease in the acidity of the adsorption system ($pH > pH_{pzc}$) greatly improved the adsorbents' adsorption capacity. For instance, the adsorption capacity was raised from 0 to 18.34 mg/g just by a single unit increase in the solution pH (from pH 2.0 to pH 3.0). Subsequent and progressive single unit-wise increases in the solution pH close to and beyond the pH_{pzc} always resulted in more than 50% improvement in the adsorption capacity until the attainment of a maximum at pH 6.0 (optimum pH for this study). Notably, the pH variation studies were terminated at pH 6.0, as the author had initially recorded insignificant adsorption at alkaline

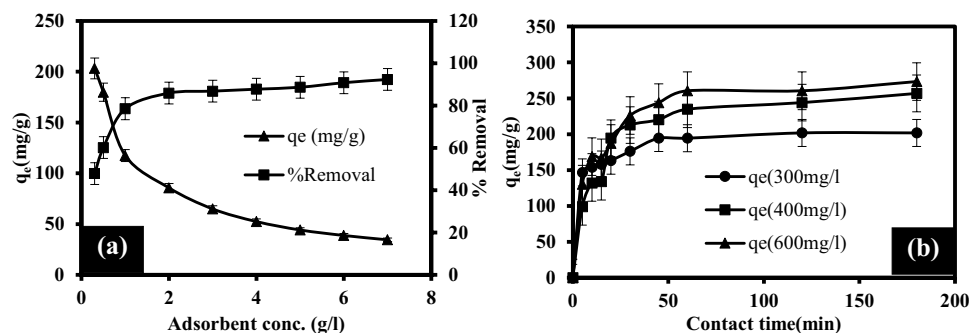
pH regions due to possible precipitation of the zinc cation to its hydroxide analogue.

Effect of adsorbent dosage

The variation in the adsorption capacity (mg/g) and removal efficiency (%) of 'MA' due to the amount of adsorbent used (dosage, g/L) was simultaneously investigated. According to the result presented in Fig. 7a, the adsorption capacity was found to vary inversely to the removal efficiency. Meanwhile, Igwegbe et al. (2020b) has reported a strong dependence of removal efficiency on the adsorbates' initial concentration; hence, their values may not provide an accurate reflection of the sorption ability of a given adsorbent. Therefore, our discussion here only emphasized the relationship between that adsorbent dosage and adsorption capacity (which provides a better reflection of the adsorbents' intrinsic adequacy) (Igwegbe et al. 2020b; Oba et al. 2021; Aniagor et al. 2021a).

Figure 7a generally depicts a steady decline in the adsorption capacity as the adsorbent dosage increased from 0.3 to 7.0 g/L. Although a general decline in the adsorption capacity was observed as the adsorbent dosage increased, the extent was particularly dependent on the adsorbent mass ratio at a given time (Aniagor et al. 2021b; Mohamed et al. 2021). For instance, a 0.2 g/L increase in the adsorbent dosage (that is from 0.3 to 0.5 g/L) resulted in about a 12% loss of adsorption capacity, while a 0.5 g/L increase (that is from

Fig. 7 **a** Combined effect of adsorbent dose on adsorption capacity and removal efficiency, **b** effect of contact time on the adsorption capacity at varying initial adsorbate concentrations (error bars represent \pm standard experimental errors)



0.5 to 1.0 g/L) showed about 35% adsorption capacity loss. A similar observation which is related to the progressive saturation and eventual clogging of the adsorption sites, thus limiting zinc ions adsorption, was made at higher adsorbent dosages (Hashem et al. 2020a; Hashem and Aniagor 2021). Hence, the maximum adsorption capacity for this study was recorded at a 0.3 g/L adsorbent dosage.

Effect of adsorption time

Figure 7b presents the combined plot of contact time and initial concentration effect on the adsorption capacity. The amount adsorbed generally improved as the adsorption time extended and as the initial adsorbate concentration increased. Meanwhile, a rapid uptake was witnessed within the first 10 min of adsorption, as the respective amount of zinc ion adsorbed was strongly dependent on the initial adsorbate concentration. Within this initial adsorption stage (first 10 min), about 80% of the optimum adsorption capacity for this study was realized. This occurrence could be due to the huge availability of active sites and the high solute (zinc ion) concentration gradient which offered a substantial driving force for favourable uptake (Zhuang et al. 2020; Zhuang and Wang 2019). As the adsorption time extended (beyond 10 min), the solute uptake amounts progressively diminished until the attainment of equilibrium at 120 min. The adsorption capacity reduction as contact time extended is due to the progressive saturation of the adsorption sites, thus limiting the uptake of more solutes (Guo and Wang 2019). A similar equilibrium time as that obtained in this study has been previously reported by other authors that

employed cellulose-based adsorbents in the uptake of different metal cations (Ebrahimi et al. 2015; Hashem et al. 2020a, c).

Adsorption modelling

Isotherm studies

The adsorbate concentration effect of the equilibrium adsorption data was fitted to different isotherm models whose equations are depicted in Table S1. The evaluated model parameters and their R^2 -values are presented in Table 1, while the experimental dataset was presented as a plot in Fig. 8. Meanwhile, the insufficiency of the application R^2 -value alone for the determination of the best-fit non-linear model has been highlighted (Abonyi et al. 2019). As a result, seven (7) error models, whose equations are presented in Table S3, were applied for determining the best-fit isotherm model. To limit the inconsistencies often experienced during the application of multiple error models (as was the case in this study), a process of normalizing the different error values from the error models for a given isotherm was adopted (Aniagor et al. 2021c). Consequently, only the sum of the normalized error (SNE) value will be considered during the isotherm modelling discussion and the lower the SNE value (as shown in Table S4), the better the model fits the experimental isotherm data. The error values and the corresponding SNE for all the isotherm models are depicted in Table S4.

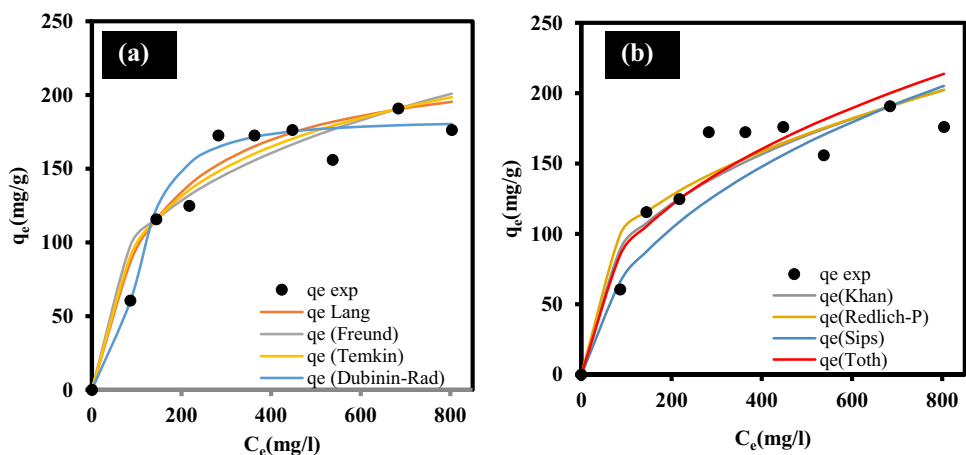
The Sips model is considered the overall best fit since it returned the lowest SNE value of 1.0498 and an appreciably high R^2 value. As a hybrid model, Sip isotherm bridges the homogeneous monolayer and heterogeneous

Table 1 Isotherm model parameters

2-parameter models			
Langmuir	Freundlich	Temkin	D-R*
$q_{\max} = 229.985$	$n_F = 3.109$	$A_T = 7.6E-02$	$q_o = 182.656$
$K_L = 1.6134$	$K_F = 23.371$	$b_T = 52.219$	$B_0 = 1.3E-03$
$R_L = 7.0E-03$	$R^2 = 0.983$	$R^2 = 0.987$	$R^2 = 0.993$
$R^2 = 0.990$	$SNE = 1.0611$	$SNE = 1.0672$	$SNE = 1.0714$
$SNE = 1.0704$			
3-parameter models			
Khan	R-P*	Sips	Toth
$q_{\max} = 2.125$	$k_g = 29.109$	$K_S = 4.970$	$k_T = 13.592$
$b_K = 303.079$	$\alpha_R = -0.127$	$\alpha_S = 6.1E-03$	$\alpha_T = 9.0E-02$
$\alpha_K = 0.633$	$g = 0.195$	$\beta_S = 0.600$	$1/t = 0.588$
$R^2 = 0.982$	$R^2 = 0.981$	$R^2 = 0.971$	$R^2 = 0.981$
$SNE = 1.0600$	$SNE = 1.0590$	$SNE = 1.0498$	$SNE = 1.0558$

*D-R Dubinin–Radushkevich; R-P Redlich–Peterson

Fig. 8 The isotherm plot for **a** 2-parameter models, **b** 3-parameter model



multilayer postulations of the Langmuir and Freundlich models, respectively. At low adsorbate concentration, the Sips model tilt towards the Freundlich model and conversely favours the Langmuir model at high concentration. The Freundlich constant ‘*n*’ (adsorbate–adsorbent affinity index) value which is greater than unity indicates favourable adsorption (Liu et al. 2018), which occurred mostly at low adsorbate concentration.

The magnitude of the D-R mean energy (*E*, KJ/mol) is often applied to classifying the nature of a given adsorption system (Hashem et al. 2022). The physical and chemical nature of an adsorption system is, respectively, implied at *E* < 8 kJ/mol and *E* > 8 kJ/mol (Dada et al. 2012). By applying Eq. (8), a D-R mean energy value of 0.382 kJ/mol (*E* < 8 kJ/mol) was obtained in this study. Hence, the occurrence of physical adsorption, with electrostatic interaction between the adsorbate and adsorbent, which was further confirmed in "Adsorbent comparison", is thus postulated (Wang et al. 2013).

$$E = \frac{1}{\sqrt{2\beta_D}}, \tag{8}$$

The Langmuir model also showed a maximum adsorption capacity of 229.985 mg/g and a favourability index (*R_L*) of 7.0E–03, which is indicative of a favourable adsorption process. The positive Temkin isotherm constant (*b_T*) recorded in this study implies a favourable sorption process. Furthermore, the heterogeneity of the Zn(II) ion adsorption system was further confirmed by the Redlich-Peterson *g*-values of 0.195, which is approaching zero. Judging from the SNE values, the best-fitted adsorption isotherm models in their descending order are Sips > Toth > Redlich–Peterson > Khan > Freundlich > Temkin > Langmuir > Dubinin–Radushkevich.

Kinetic studies

As already explained in "Isotherm studies", only the sum of normalized error (SNE) value will be considered in the discussions on kinetic studies, and the lower the SNE value (as shown in Table 2), the better the kinetic model fit. The error values and the corresponding SNE values for all the kinetic models are depicted in Table S5. The Elovich (SNE = 1.0429), intraparticle diffusion (SNE = 1.0205) and pseudo-first order (SNE = 1.0455) provided the best fitting for 200, 400 and 600 mg/L adsorption systems, respectively. Similarly, the plot of the different kinetic models is presented in Fig. 9.

Despite the emergence of the respective best-fit models, the relatively low SNE value (≤ 1.0872) and high *R*²-values (≥ 0.92) were recorded for all models applied in the modelling of the entire adsorption system (200, 400 and 600 mg/L) showing their good fitting to the experimental dataset. Studies (Wang et al. 2020; Delgado et al. 2019) have shown that PFO usually provides a better fit at high initial adsorbate concentration, where the ratio of adsorbate ions is higher compared to the available active sites. This assertion supports the emergence of PFO as the best-fit model for the 600 mg/L adsorption system. Meanwhile, the linear dependence of its rate constant (*k₁*) on the initial Zn (II) ion concentration has been highlighted (Wang et al. 2020). The values of the adsorption rate constant recorded for the PFO model (which ranges from 0.0683 to 0.155) (Table 2) were in all cases greater than those obtained for PSO, thus emphasizing the superiority of PFO model prediction to that of PSO in this study. The Elovich model postulates the heterogeneity of an adsorbent’s surface and a direct variation between the adsorption duration and activation energy (Aniagor and Menkiti 2019). The model also depicted a low desorption constant (*β*) value in the range

Table 2 Kinetic model parameters

	Pseudo-first order	Pseudo-second order	Elovich	Bangham	Intraparticle diffusion
<i>200 mg/L</i>					
$q_e = 195.755$	$q_e = 205.482$	$\alpha = 100$	$q_e = 226.263$	$k_{id} = 6.118$	
$k_1 = 0.155$	$k_2 = 1.4E-03$	$\beta = 0.024$	$k_b = 0.634$	$C = 134.767$	
$R^2 = 0.990$	$R^2 = 0.997$	$R^2 = 0.980$	$n = 0.254$	$R^2 = 0.997$	
$SNE = 1.0556$	$SNE = 1.0853$	$SNE = 1.0429$	$R^2 = 0.999$	$SNE = 1.0872$	
			$SNE = 1.1676$		
<i>400 mg/L</i>					
$q_e = 236.602$	$q_e = 269.533$	$\alpha = 76.389$	$q_e = 258.852$	$k_{id} = 30.317$	
$k_1 = 0.0817$	$k_2 = 4.2E-04$	$\beta = 0.021$	$k_b = 0.172$	$C = 0.01$	
$R^2 = 0.994$	$R^2 = 0.996$	$R^2 = 0.992$	$n = 0.641$	$R^2 = 0.922$	
$SNE = 1.0645$	$SNE = 1.0642$	$SNE = 1.0599$	$R^2 = 0.997$	$SNE = 1.0205$	
			$SNE = 1.0744$		
<i>600 mg/L</i>					
$q_e = 260.600$	$q_e = 283.808$	$\alpha = 100.00$	$q_e = 276.077$	$k_{id} = 11.773$	
$k_1 = 0.0683$	$k_2 = 4.8E-04$	$\beta = 0.020$	$k_b = 0.264$	$C = 131.564$	
$R^2 = 0.988$	$R^2 = 0.997$	$R^2 = 0.994$	$n = 0.549$	$R^2 = 0.988$	
$SNE = 1.0455$	$SNE = 1.0764$	$SNE = 1.0675$	$R^2 = 0.998$	$SNE = 1.0462$	
			$SNE = 1.0733$		

of 0.020–0.024 (Table 2), which implies improved zinc ion sorption onto ‘MA’ for all adsorption systems. Notably, the value of intraparticle (c value) recorded for the 400 mg/L system was extraordinarily low (0.01) and it implies a negligible boundary layer effect within such a system. Conversely, the occurrence of greater boundary layer effects was observed for 200 and 600 mg/L adsorption systems, as informed by their large c -values of 134.767 and 131.564, respectively (Table 2).

Thermodynamics studies

The effect of temperature on the adsorbent–adsorbate interaction during zinc ion uptake is elucidated by the adsorption thermodynamics parameters (standard free energy, ΔG° , standard enthalpy, ΔH° , and standard entropy, ΔS°). The magnitude and sign convention of these thermodynamics parameters are key to explaining the various temperature effects. For instance, the ΔG° value expresses the feasibility and spontaneity of the adsorption system, the ΔS° value informs the degree of disorderliness of the system and the ΔH° value is related to the heat content and energetic transfer within the adsorption system. The aforementioned thermodynamics parameters are evaluated accordingly from Eq. (9), while K_c is evaluated from Eq. (10).

$$\ln K_c = \frac{\Delta S^\circ}{R} - \frac{\Delta H^\circ}{RT}, \quad (9)$$

$$K_c = \frac{C_o - C_e}{C_o}, \quad (10)$$

where R is the universal gas constant (8.314 J/mol K) and T is the temperature (K). The parameters presented in Table 3 shows positive ΔG° values and negative ΔS° value, thus implying a non-spontaneous and less energetic nature of the process, respectively. According to Saha and Chowdhury (2011), such observation suggests the temperature dependence of the ‘MA’ active sites and underscores the need for the application of external energy to the system. The positive ΔH° values obtained in this study provide further confirmation of the endothermicity of the adsorption process. Also, the relatively large ΔH° value obtained in this study is well within the physicochemical adsorption range and could be related to the strong bond obtainable from the sample carboxylic and carbonyl groups on the ‘MA’.

Adsorption mechanism

The probable adsorption mechanism involved in the sorption of zinc ions onto ‘MA’ is discussed as follows:

- ion exchange and electrostatic interaction* This interaction resulted mainly from the chemical bonds formed between negatively charged functional groups of the adsorbent and the positively charged Zn (II) ions [see Eqs. (6) and (7)]. This mechanism is predominant when the $\text{pH} > \text{pH}_{\text{PZC}}$. The oxygenous (carboxylate, carbonyl, and hydroxyl) surface groups of ‘MA’ were primarily responsible for the electrostatic interactions at favourable solution pH.
- Electron donor–acceptor interaction*: Due to the presence of H-donor functional groups (–OH and –

Fig. 9 The respective kinetic plots for PFO, PSO, Intraparticle diffusion, Elovich and Bangham model

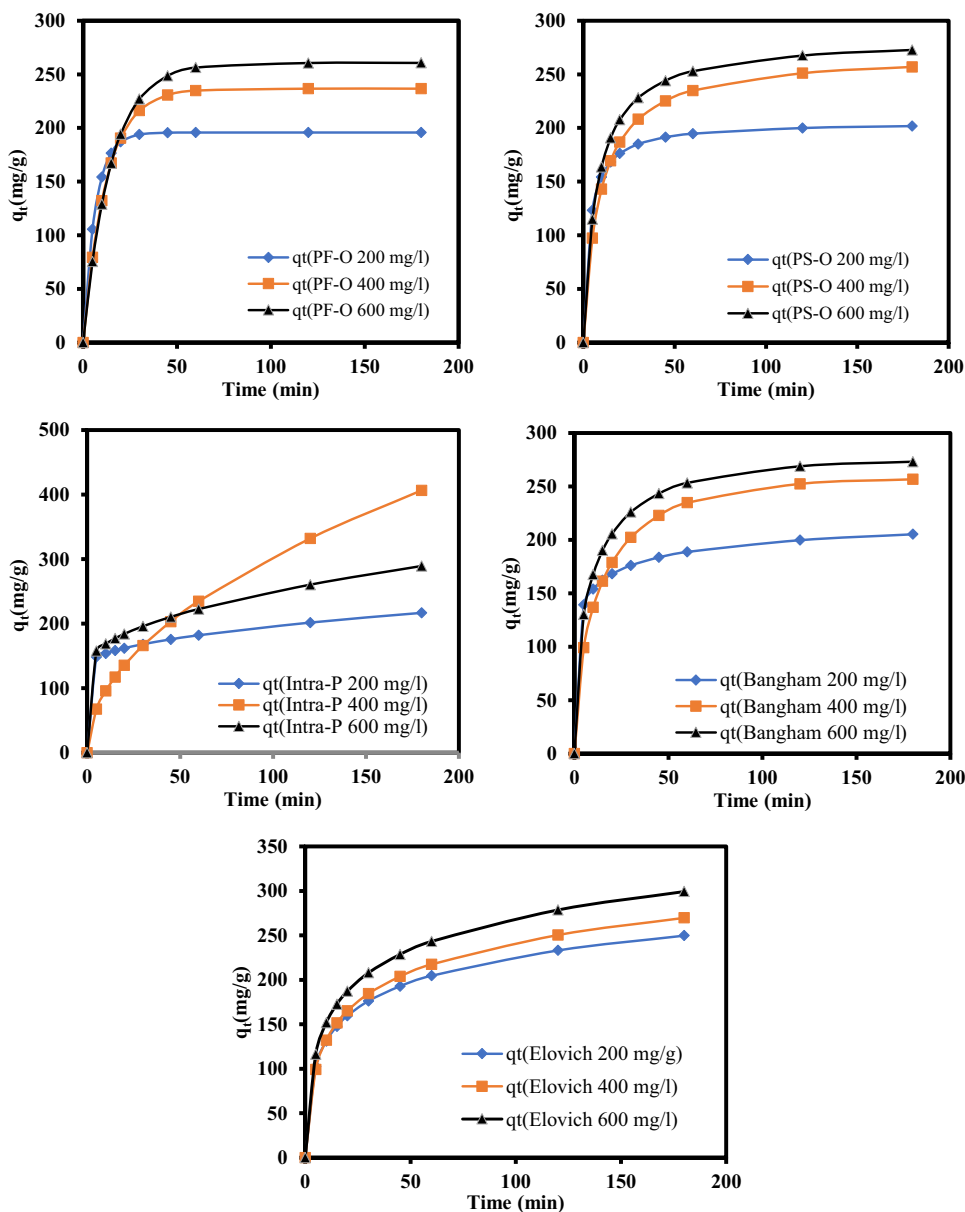
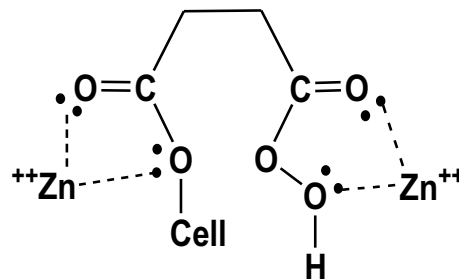


Table 3 Thermodynamic parameters

Temp. (K)	ΔG° (KJ mol ⁻¹)	ΔH° (KJ mol ⁻¹)	ΔS° (JK ⁻¹ mol ⁻¹)
30	9.276		
50	11.378	61.241	- 4.875
60	12.494		

COOH) on ‘MA’, the mechanism of adsorption could be based on the complexation between the metal ion and the anionic MA-COO⁻ conjugate (H-acceptor) (Scheme 1). Also, the carbonyl groups of ‘MA’ can engage in donor-acceptor interaction, during which the carbonyl groups of stronger dipole moment could



Scheme 1 Proposed mechanism for zinc ion adsorption onto ‘MA’

donate the electron which would be accepted by the adsorbate (Mattson et al. 1969).

Table 4 Comparison of adsorption capacities of various organic acid-modified sorbents

Adsorbent	Adsorbate	Adsorption capacity (mg/g)	References
Chemically modified sawdust	Pb(II)	304.0	Salazar-Rabago and Leyva-Ramos (2016)
Modified <i>Alhagi graecorum</i> root residue	Zn(II)	229.98	Present study
monosodium glutamate-modified rubber leaf powder	Pb(II)	109.95	Fadzil et al. (2016)
Citric acid-modified rubber leaf powder	Pb(II)	97.19	Fadzil et al. (2016)
*EDTA-modified jack fruit peel	Ni(II)	52.08	Ranasinghe et al. (2018)
*EDTA-modified jack fruit peel	Cr(III)	41.67	Ranasinghe et al. (2018)
**SDS-modified jack fruit peel	Cr(III)	26.25	Ranasinghe et al. (2018)
**SDS-modified jack fruit peel	Ni(II)	20.88	Ranasinghe et al. (2018)
Citric acid-modified cellulose nanofibrous mats	Cr(VI)	13.30	Zhang et al. (2020)

*EDTA ethylenediaminetetraacetic acid

**SDS sodium dodecyl sulphate

Adsorbent comparison

The 'MA' adsorption capacity for the uptake of Zn(II) was compared to those of similar adsorbents reported in the literature for heavy metal adsorption. The findings from the comparison are presented in Table 4. The adsorption capacity of 'MA' was, however, found to be higher than that of most adsorbents considered in the comparison. This is an indication of the effectiveness of 'MA' for the uptake of aqueous Pb(II).

Conclusions

A novel biosorbent, with high carboxyl content, was synthesized via the esterification reaction between highly cellulosic *Alhagi* root material (AG) and succinic acid. The novel biosorbent was effective for aqueous zinc ion uptake. Using different adsorbent characterization tools (SEM, EDX, FTIR and pH_{pzc} analyses) the acidic nature of 'MA' and its textural characteristics were explained. The equilibrium and kinetic characteristics suggested a hybrid mix of monolayer–multilayer adsorption and intraparticle diffusion-controlled chemisorption, respectively. The entire sorption process was pH responsive, while electrostatic and electro-donor–acceptor interaction was established as the major uptake mechanism. Based on experimental findings, 'MA' has proven to be an excellent adsorbent for the removal due to the nature of its surface functional groups.

Supplementary Information The online version contains supplementary material available at <https://doi.org/10.1007/s40899-023-00840-3>.

Authors contributions COA contributed to conceptualization, data curation, formal analysis, investigation, validation and writing—original draft, review and editing. DMH and SF performed data curation,

formal analysis, visualization, validation and supervision. AH was involved in data curation, formal analysis, visualization, validation, supervision and writing—original draft, review and editing.

Funding No funding was available for this research.

Availability of data and materials All data generated or analysed during this study are included in this manuscript draft.

Declarations

Conflict of interest The authors declare that there is no known competing interest.

Ethical approval This work does not contain any data from human participants or animals. The authors, therefore, claim compliance with the ethical standards.

Consent to participate This is not applicable, as this study does not involve human subjects.

Consent to publish This is not applicable, as this study does not involve human subjects.

References

- Abdelraheem WH, Rabia MK, Ismail NM (2016) Evaluation of copper speciation in the extract of *Eichhornia crassipes* using reverse and forward/CLE voltammetric titrations. Arab J Chem 9:S1670–S1678
- Abdelraheem WH, Komy ZR, Ismail NM (2017) Electrochemical determination of Cu²⁺ complexation in the extract of *E. crassipes* by anodic stripping voltammetry. Arab J Chem 10:S1105–S1110
- Abonyi M, Aniagor C, Menkiti M (2019) Effective dephenolation of effluent from petroleum industry using ionic-liquid-induced hybrid adsorbent. Arab J Sci Eng 44(12):10017–10029
- Adigun O, Oninla V, Babarinde NA (2019) Application of sugarcane leaves as biomass in the removal of cadmium (II), lead (II) and zinc (II) ions from polluted water. Int J Energy Water Resour 3(2):141–152

- Ahmad MF, Haydar S, Quraishi TA (2013) Enhancement of biosorption of zinc ions from aqueous solution by immobilized *Candida utilis* and *Candida tropicalis* cells. *Int Biodeter Biodegrad* 83:119–128
- Ali I, Alharbi OM, Allothman ZA, Badjah AY (2018) Kinetics, thermodynamics, and modeling of amido black dye photodegradation in water using Co/TiO₂ nanoparticles. *Photochem Photobiol* 94(5):935–941
- Ali I, Alharbi OM, AlOthman ZA, Alwarthan A, Al-Mohaimed AM (2019) Preparation of a carboxymethylcellulose-iron composite for uptake of atorvastatin in water. *Int J Biol Macromol* 132:244–253
- Al-Shaalan NH, Ali I, AlOthman ZA, Al-Wahaibi LH, Alabdulmonem H (2019) High performance removal and simulation studies of diuron pesticide in water on MWCNTs. *J Mol Liq* 289:111039
- Aniagor C, Menkiti M (2018) Kinetics and mechanistic description of adsorptive uptake of crystal violet dye by lignified elephant grass complexed isolate. *J Environ Chem Eng* 6(2):2105–2118
- Aniagor C, Menkiti M (2019) Synthesis, modification and use of lignified bamboo isolate for the renovation of crystal violet dye effluent. *Appl Water Sci* 9(4):77
- Aniagor CO, Menkiti MC (2020) Relational description of an adsorption system based on isotherm, adsorption density, adsorption potential, hopping number and surface coverage. *Sigma* 38(3):1073–1098
- Aniagor CO, Igwegbe CA, Ighalo JO, Oba SN (2021a) Adsorption of doxycycline from aqueous media: a review. *J Mol Liq*. <https://doi.org/10.1016/j.molliq.2021.116124>
- Aniagor CO, Elshkankery M, Fletcher A, Morsy OM, Abdel-Halim E, Hashem A (2021b) Equilibrium and kinetic modelling of aqueous cadmium ion and activated carbon adsorption system. *Water Conserv Sci Eng* 6:95–104
- Aniagor CO, Afifi M, Hashem A (2021c) Heavy metal adsorptive application of hydrolyzed corn starch. *J Polym Res* 28(11):1–10
- Awual MR (2016) Solid phase sensitive palladium (II) ions detection and recovery using ligand based efficient conjugate nanomaterials. *Chem Eng J* 300:264–272
- Awual MR, Alharthi NH, Hasan MM, Karim MR, Islam A, Znad H, Hossain MA, Halim ME, Rahman MM, Khaleque MA (2017) Inorganic-organic based novel nano-conjugate material for effective cobalt (II) ions capturing from wastewater. *Chem Eng J* 324:130–139
- Awual MR, Hasan MM, Asiri AM, Rahman MM (2019a) Novel optical composite material for efficient vanadium (III) capturing from wastewater. *J Mol Liq* 283:704–712
- Awual MR, Hasan MM, Islam A, Rahman MM, Asiri AM, Khaleque MA, Sheikh MC (2019b) Offering an innovative composited material for effective lead (II) monitoring and removal from polluted water. *J Clean Prod* 231:214–223
- Badruddoza AZM, Shawon ZBZ, Tay WJD, Hidajat K, Uddin MS (2013) Fe₃O₄/cyclodextrin polymer nanocomposites for selective heavy metals removal from industrial wastewater. *Carbohydr Polym* 91(1):322–332
- Barakat M (2011) New trends in removing heavy metals from industrial wastewater. *Arab J Chem* 4(4):361–377
- Chen X, Lv F, Lin Y, Wang Z, Meng L, Zhang Q, Zhang W, Li L (2018) Structure evolution of polyethylene-plasticizer film at industrially relevant conditions studied by in-situ X-ray scattering: the role of crystal stress. *Eur Polym J* 101:358–367
- Dada A, Olalekan A, Olatunya A, Dada O (2012) Langmuir, Freundlich, Temkin and Dubinin-Radushkevich isotherms studies of equilibrium sorption of Zn²⁺ onto phosphoric acid modified rice husk. *IOSR J Appl Chem* 3(1):38–45
- Delgado N, Capparelli A, Navarro A, Marino D (2019) Pharmaceutical emerging pollutants removal from water using powdered activated carbon: study of kinetics and adsorption equilibrium. *J Environ Manage* 236:301–308
- Ebrahimi A, Ehteshami M, Dahrazma B (2015) Isotherm and kinetic studies for the biosorption of cadmium from aqueous solution by *Alhaji maurorum* seed. *Process Saf Environ Prot* 98:374–382
- Fadzil F, Ibrahim S, Hanafiah MAKM (2016) Adsorption of lead (II) onto organic acid modified rubber leaf powder: batch and column studies. *Process Saf Environ Prot* 100:1–8
- Foo KY, Hameed BH (2010) Insights into the modeling of adsorption isotherm systems. *Chem Eng J* 156(1):2–10
- Freundlich H (1907) Über die adsorption in lösungen. *Z Phys Chem* 57(1):385–470
- Guo X, Wang J (2019) A general kinetic model for adsorption: theoretical analysis and modeling. *J Mol Liq* 288:111100
- Hashem A, Badawy SM (2015) *Sesbania sesban* L. biomass as a novel adsorbent for removal of Pb (II) ions from aqueous solution: non-linear and error analysis. *Green Process Synth* 4(3):179–190
- Hashem A, Hussein HA, Sanousy MA, Adam E, Saad EE (2011) Monomethylolated thiourea-sawdust as a new adsorbent for removal of Hg (II) from contaminated water: equilibrium kinetic and thermodynamic studies. *Polym-Plast Technol Eng* 50(12):1220–1230
- Hashem A, Al-Anwar A, Nagy NM, Hussein DM, Eisa S (2016) Isotherms and kinetic studies on adsorption of Hg (II) ions onto *Ziziphus spina-christi* L. from aqueous solutions. *Green Process Synth* 5(2):213–224
- Hashem A, Badawy S, Farag S, Mohamed L, Fletcher A, Taha G (2020a) Non-linear adsorption characteristics of modified pine wood sawdust optimised for adsorption of Cd (II) from aqueous systems. *J Environ Chem Eng* 8:103966
- Hashem A, Nasr M, Fletcher A, Mohamed LA (2020b) Aminated acrylic fabric waste derived sorbent for Cd (II) ion removal from aqueous solutions: mechanism, equilibria and kinetics. *J Polym Environ* 29:1–12
- Hashem A, Fletcher A, Younis H, Mauof H, Abou-Okeil A (2020c) Adsorption of Pb (II) ions from contaminated water by 1, 2, 3, 4-butanetetracarboxylic acid-modified microcrystalline cellulose: isotherms, kinetics, and thermodynamic studies. *Int J Biol Macromol* 164:3193–3203
- Hashem A, Aniagor C, Hussein D, Farag S (2021) Application of novel butane-1, 4-dioic acid-functionalized cellulosic biosorbent for aqueous cobalt ion sequestration. *Cellulose* 28(6):3599–3615
- Hashem A, Aniagor CO, Nasr M, Abou-Okeil A (2021) Efficacy of treated sodium alginate and activated carbon fibre for Pb(II) adsorption. *Int J Biol Macromol*. <https://doi.org/10.1016/j.ijbmac.2021.02.067>
- Hashem A, Aniagor CO, Morsy OM, Abou-Okeil A, Aly A (2022) Apricot seed shell: an agro-waste biosorbent for acid blue193 dye adsorption. *Biomass Convers Biorefinery*:1–14
- Huang W, Hu Y, Li Y, Zhou Y, Niu D, Lei Z, Zhang Z (2018) Citric acid-crosslinked β -cyclodextrin for simultaneous removal of bisphenol A, methylene blue and copper: the roles of cavity and surface functional groups. *J Taiwan Inst Chem Eng* 82:189–197
- Ighalo JO, Tijani IO, Ajala J, Ayandele FO, Eletta O, Adeniyi AG (2020) Competitive biosorption of Pb (II) and Cu (II) by functionalised micropogonias undulates scales. *Recent Innov Chem Eng* 13:1–12
- Igwegbe CA, Onukwuli OD, Ighalo JO, Okoye PU (2020a) Adsorption of cationic dyes on *Dacryodes edulis* seeds activated carbon modified using phosphoric acid and sodium chloride. *Environ Process* 7(4):1151–1171
- Igwegbe CA, Oba SN, Aniagor CO, Adeniyi AG, Ighalo JO (2020b) Adsorption of ciprofloxacin from water: a comprehensive review. *J Industr Eng Chem* 93(57):77
- Jagaba A, Kutty S, Khaw S, Lai C, Isa M, Baloo L, Lawal I, Abubakar S, Umaru I, Zango Z (2020) Derived hybrid biosorbent for zinc


- (II) removal from aqueous solution by continuous-flow activated sludge system. *J Water Process Eng* 34:101152
- Kapoor A, Yang R (1989) Correlation of equilibrium adsorption data of condensable vapours on porous adsorbents. *Gas Sep Purif* 3(4):187–192
- Khair U, Fahmi H, Al Hakim S, Rahim R (2017) Forecasting error calculation with mean absolute deviation and mean absolute percentage error. *J Phys Conf Ser* 930:012002
- Khalil M, Hashem A, Hebeish A (1990) Carboxymethylation of maize starch. *Starch-Stärke* 42(2):60–63
- Khan A, Ataullah R, Al-Haddad A (1997) Equilibrium adsorption studies of some aromatic pollutants from dilute aqueous solutions on activated carbon at different temperatures. *J Colloid Interface Sci* 194(1):154–165
- King P, Anuradha K, Lahari SB, Kumar YP, Prasad V (2008) Biosorption of zinc from aqueous solution using *Azadirachta indica* bark: equilibrium and kinetic studies. *J Hazard Mater* 152(1):324–329
- Komy ZR, Abdelraheem WH, Ismail NM (2013) Biosorption of Cu^{2+} by *Eichhornia crassipes*: Physicochemical characterization, biosorption modeling and mechanism. *J King Saud Univ Sci* 25(1):47–56
- Kumar KV, Porkodi K, Rocha F (2008) Comparison of various error functions in predicting the optimum isotherm by linear and non-linear regression analysis for the sorption of basic red 9 by activated carbon. *J Hazard Mater* 150(1):158–165
- Langmuir I (1916) The constitution and fundamental properties of solids and liquids. Part I. Solids. *J Am Chem Soc* 38(11):2221–2295
- Li D, Henschen J, Ek M (2017) Esterification and hydrolysis of cellulose using oxalic acid dihydrate in a solvent-free reaction suitable for preparation of surface-functionalised cellulose nanocrystals with high yield. *Green Chem* 19(23):5564–5567
- Liu X, Chen Z-Q, Han B, Su C-L, Han Q, Chen W-Z (2018) Biosorption of copper ions from aqueous solution using rape straw powders: optimization, equilibrium and kinetic studies. *Ecotoxicol Environ Saf* 150:251–259
- Luef E, Prey T, Kubicek CP (1991) Biosorption of zinc by fungal mycelial wastes. *Appl Microbiol Biotechnol* 34(5):688–692
- Marquardt DW (1963) An algorithm for least-squares estimation of nonlinear parameters. *J Soc Ind Appl Math* 11(2):431–441
- Matouq M, Jildeh N, Qtaishat M, Hindiyyeh M, AlSyoub MQ (2015) The adsorption kinetics and modeling for heavy metals removal from wastewater by *Moringa* pods. *J Environ Chem Eng* 3(2):775–784
- Mattson JA, Mark HB Jr, Malbin MD, Weber WJ Jr, Crittenden JC (1969) Surface chemistry of active carbon: specific adsorption of phenols. *J Colloid Interface Sci* 31(1):116–130
- Menkiti M, Aniagor C (2018) Parametric studies on descriptive isotherms for the uptake of crystal violet dye from aqueous solution onto lignin-rich adsorbent. *Arab J Sci Eng* 43(5):2375–2392
- Menkiti M, Abonyi M, Aniagor C (2018a) Process equilibrium, kinetics, and mechanisms of ionic-liquid induced dephenolation of petroleum effluent. *Water Conserv Sci Eng* 3(3):205–220
- Menkiti M, Aniagor C, Agu C, Ugonabo V (2018b) Effective adsorption of crystal violet dye from an aqueous solution using lignin-rich isolate from elephant grass. *Water Conserv Sci Eng* 3(1):33–46
- Mohamed LA, Aniagor CO, Taha GM, Abou-Okeil A, Hashem A (2021) Mechanistic investigation of the mass transfer stages involved during the adsorption of aqueous lead onto *Scopulariopsis brevicompactum* fungal biomass. *Environ Chall* 5:100373
- Ng J, Cheung W, McKay G (2002) Equilibrium studies of the sorption of Cu (II) ions onto chitosan. *J Colloid Interface Sci* 255(1):64–74
- Noh JS, Schwarz JA (1990) Effect of HNO_3 treatment on the surface acidity of activated carbons. *Carbon* 28(5):675–682
- Oba SN, Ighalo JO, Aniagor CO, Igwegbe CA (2021) Removal of ibuprofen from aqueous media by adsorption: a comprehensive review. *Sci Total Environ*. <https://doi.org/10.1016/j.scitotenv.2021.146608>:p.146608
- Paduraru C, Tofan L, Teodosiu C, Bunia I, Tudorachi N, Toma O (2015) Biosorption of zinc (II) on rapeseed waste: equilibrium studies and thermogravimetric investigations. *Process Saf Environ Prot* 94:18–28
- Ranasinghe S, Navaratne A, Priyantha N (2018) Enhancement of adsorption characteristics of Cr (III) and Ni (II) by surface modification of jackfruit peel biosorbent. *J Environ Chem Eng* 6(5):5670–5682
- Redlich O, Peterson DL (1959) A useful adsorption isotherm. *J Phys Chem* 63(6):1024–1024
- Rivas F, Beltrán F, Gimeno O, Frades J, Carvalho F (2006) Adsorption of landfill leachates onto activated carbon: equilibrium and kinetics. *J Hazard Mater* 131(1–3):170–178
- Saha P, Chowdhury S (2011) Insight into adsorption thermodynamics. *Thermodynamics* 16:349–364
- Salazar-Rabago J, Leyva-Ramos R (2016) Novel biosorbent with high adsorption capacity prepared by chemical modification of white pine (*Pinus durangensis*) sawdust. *Adsorption of Pb (II) from aqueous solutions*. *J Environ Manag* 169:303–312
- Sasmal S, Goud VV, Mohanty K (2012) Characterization of biomasses available in the region of North-East India for production of bio-fuels. *Biomass Bioenerg* 45:212–220
- Sayahi H, Asadabadi S (2022) Anchoring carboxylated pineapple peel cellulose and EDTA onto magnetic (3-aminopropyl) triethoxysilane to effective removal of copper (II) and zinc (II) from polluted water. *Cellulose* 30:1–23
- Schweitzer L, Noblet J (2018) Water contamination and pollution. *Green Chem*. <https://doi.org/10.1016/b978-0-12-809270-5.00011-x>
- Serguchev YA, Beletskaya IP (1980) Oxidative decarboxylation of carboxylic acids. *Russ Chem Rev* 49(12):1119
- Shahat A, Hassan HM, El-Shahat M, El Shahawy O, Awwal MR (2018a) Visual nickel (II) ions treatment in petroleum samples using a mesoporous composite adsorbent. *Chem Eng J* 334:957–967
- Shahat A, Hassan HM, Azzazy HM, El-Sharkawy E, Abdou HM, Awwal MR (2018b) Novel hierarchical composite adsorbent for selective lead (II) ions capturing from wastewater samples. *Chem Eng J* 332:377–386
- Temkin M (1940) Kinetics of ammonia synthesis on promoted iron catalysts. *Acta Physiochim URSS* 12:327–356
- Toth J (1971) State equation of the solid-gas interface layers. *Acta Chim Hung* 69:311–328
- Vargas AM, Cazetta AL, Martins AC, Moraes JC, Garcia EE, Gauze GF, Costa WF, Almeida VC (2012) Kinetic and equilibrium studies: adsorption of food dyes Acid Yellow 6, Acid Yellow 23, and Acid Red 18 on activated carbon from flamboyant pods. *Chem Eng J* 181:243–250
- Wang XS, Qin Y, Li ZF (2006) Biosorption of zinc from aqueous solutions by rice bran: kinetics and equilibrium studies. *Sep Sci Technol* 41(4):747–756
- Wang G, Chang Q, Zhang M, Han X (2013) Effect of pH on the removal of Cr (III) and Cr (VI) from aqueous solution by modified polyethyleneimine. *React Funct Polym* 73(11):1439–1446
- Wang L, Shi C, Pan L, Zhang X, Zou J-J (2020) Rational design, synthesis, adsorption principles and applications of metal oxide adsorbents: a review. *Nanoscale* 12(8):4790–4815
- Wołowicz M, Komorowska-Kaufman M, Pruss A, Rzepa G, Bajda T (2019) Removal of heavy metals and metalloids from water

- using drinking water treatment residuals as adsorbents: a review. *Minerals* 9(8):487
- Yan Y, Xu X, Shi C, Yan W, Zhang L, Wang G (2019) Ecotoxicological effects and accumulation of ciprofloxacin in *Eichhornia crassipes* under hydroponic conditions. *Environ Sci Pollut Res Int* 26(29):30348–30355
- Zhang D, Xu W, Cai J, Cheng S-Y, Ding W-P (2020) Citric acid-incorporated cellulose nanofibrous mats as food materials-based biosorbent for removal of hexavalent chromium from aqueous solutions. *Int J Biol Macromol* 149:459–466
- Zhou Y, Hu Y, Huang W, Cheng G, Cui C, Lu J (2018) A novel amphoteric β -cyclodextrin-based adsorbent for simultaneous removal of cationic/anionic dyes and bisphenol A. *Chem Eng J* 341:47–57
- Zhuang S, Wang J (2019) Removal of cobalt ion from aqueous solution using magnetic graphene oxide/chitosan composite. *Environ Prog Sustain Energy* 38(s1):S32–S41
- Zhuang S, Zhu K, Wang J (2020) Fibrous chitosan/cellulose composite as an efficient adsorbent for Co (II) removal. *J Clean Prod* 285:124911

Publisher's Note Springer Nature remains neutral with regard to jurisdictional claims in published maps and institutional affiliations.

Springer Nature or its licensor (e.g. a society or other partner) holds exclusive rights to this article under a publishing agreement with the author(s) or other rightsholder(s); author self-archiving of the accepted manuscript version of this article is solely governed by the terms of such publishing agreement and applicable law.

Authors and Affiliations

Chukwunonso Onyeka Aniagor¹  · Doaa Mohamed Hussein² · Sohair Farag³ · Ali Hashem³ 

¹ Department of Chemical Engineering, Nnamdi Azikiwe University, P.M.B.5025, Awka, Nigeria

² Chemistry Department, Faculty of Science, Sebha University, Sebha, Libya

³ Institute of Textile Research and Technology, National Research Centre, Dokki, Cairo, Egypt